Scaling law describes the spin-glass response in theory, experiments and simulations

Q. Zhai,[1, *] I. Paga,[2, 3, *] M. Baity-Jesi,[4] E. Calore,[5] A. Cruz,[6, 7] L.A. Fernandez,[3, 7] J.M. Gil-Narvion,[7]
I. Gonzalez-Adalid Pemartin,[3] A. Gordillo-Guerrero,[8, 9, 7] D. Iñiguez,[7, 10] A. Maiorano,[11, 12, 7]
E. Marinari,[13, 12] V. Martin-Mayor,[3, 7] J. Moreno-Gordo,[7, 6] A. Muñoz-Sudupe,[3, 7] D. Navarro,[14]
R. L. Orbach,[1] G. Parisi,[15, 12] S. Perez-Gaviro,[16, 7, 6] F. Ricci-Tersenghi,[13, 12] J.J. Ruiz-Lorenzo,[17, 9, 7]
S.F. Schifano,[18] D. L. Schlagel,[19] B. Seoane,[3, 7] A. Tarancon,[6, 7] R. Tripiccione,[5] and D. Yllanes[20, 7, †]

[1] *Texas Materials Institute, The University of Texas at Austin, Austin, Texas 78712, USA*
[2] *Dipartimento di Fisica, Sapienza Università di Roma, INFN, Sezione di Roma 1,Italy*
[3] *Departamento de Física Teórica, Universidad Complutense, 28040 Madrid, Spain*
[4] *Eawag, Überlandstrasse 133, CH-8600 Dübendorf, Switzerland*
[5] *Dipartimento di Fisica e Scienze della Terra, Università di Ferrara e INFN, Sezione di Ferrara, I-44122 Ferrara, Italy*
[6] *Departamento de Física Teórica, Universidad de Zaragoza, 50009 Zaragoza, Spain*
[7] *Instituto de Biocomputación y Física de Sistemas Complejos (BIFI), 50018 Zaragoza, Spain*
[8] *Departamento de Ingeniería Eléctrica, Electrónica y Automática, U. de Extremadura, 10003, Cáceres, Spain*
[9] *Instituto de Computación Científica Avanzada (ICCAEx),
Universidad de Extremadura, 06006 Badajoz, Spain*
[10] *Fundación ARAID, Diputación General de Aragón, Zaragoza, Spain*
[11] *Dipartimento di Biotecnologie, Chimica e Farmacia,
Università degli studi di Siena, 53100, Siena, Italy*
[12] *INFN, Sezione di Roma 1, I-00185 Rome, Italy*
[13] *Dipartimento di Fisica, Sapienza Università di Roma, and CNR-Nanotec, I-00185 Rome, Italy*
[14] *Departamento de Ingeniería, Electrónica y Comunicaciones and I3A, U. de Zaragoza, 50018 Zaragoza, Spain*
[15] *Dipartimento di Fisica, Sapienza Università di Roma, INFN, and CNR-Nanotec, I-00185 Rome, Italy*
[16] *Escuela Universitaria Politécnica - La Almunia,
50100 La Almunia de Doña Godina, Zaragoza, Spain*
[17] *Departamento de Física, Universidad de Extremadura, 06006 Badajoz, Spain*
[18] *Dipartimento di Scienze Chimiche e Farmaceutiche,
Università di Ferrara e INFN Sezione di Ferrara, I-44122 Ferrara, Italy*
[19] *Division of Materials Science and Engineering, Ames Laboratory, Ames, Iowa 50011, USA*
[20] *Chan Zuckerberg Biohub, San Francisco, CA, 94158*

(Dated: December 1, 2020)

The correlation length ξ, a key quantity in glassy dynamics, can now be precisely measured for spin glasses both in experiments and in simulations. However, known analysis methods lead to discrepancies either for large external fields or close to the glass temperature. We solve this problem by introducing a scaling law that takes into account both the magnetic field and the time-dependent spin-glass correlation length. The scaling law is successfully tested against experimental measurements in a CuMn single crystal and against large-scale simulations on the Janus II dedicated computer.

The dynamical arrest found upon cooling glass formers (spin glasses, fragile molecular glasses, polymers, colloids, etc.) to their glass temperature T_{g} is a major open problem [1, 2]. In the longstanding description [3], this slowing down is caused by the unbounded expansion of cooperative regions as T_{g} is approached or as the system is left to age below T_{g}, which, in turn, leads to growing free-energy barriers. A quantitative description of this process is usually attempted in terms of a correlation length ξ. Unfortunately, in numerical simulations it is extremely difficult to measure the quantities that are easily accessible to experiments (and vice versa), which has led to seemingly irreconcilable approaches to the computation of the correlation length. On the one hand, theorists study correlation functions in an abstract replica

space [4–14]. On the other hand, experimentalists measure the system's response to an applied external field (either an electric field for glass-forming liquids [15] or a magnetic field for spin glasses [16–20]). Ref. [12] reconciled the two approaches by measuring the experimental response functions in a numerical simulation, but it was ultimately based on an approximate scaling law that breaks down for large fields or close to the glass temperature T_{g}. This is especially problematic, since temperatures $T \approx T_{\mathrm{g}}$ are the most relevant for the study of glass formers (ξ is restricted to a very narrow window of variation if we move away from T_{g}).

Here we are able to solve this dilemma in a framework that completely harmonizes experiments with theory. We conduct a parallel study of non-equilibrium spin-glass dynamics both in an experiment in a CuMn single crystal and in a large-scale simulation of the Ising-Edwards-Anderson (IEA) model carried out on the Janus II custom-built supercomputer [21]. We introduce

---

* These authors contributed equally to this work.
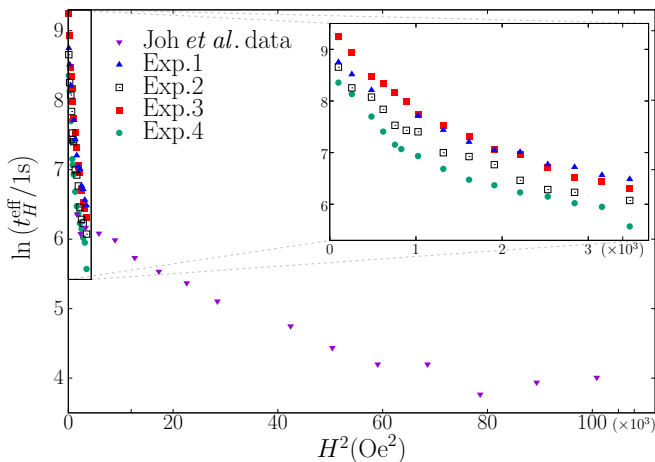† david.yllanes@czbiohub.org

FIG. 1. Comparison of the experimental situation in 1999 (data from Joh et al. [16]) and 2020 (present work). Both data sets are for $Cu_{94}Mn_6$. The 1999 data are from a poly-crystalline sample, while 2020 data come from a single crystal allowing for a much larger correlation length ξ (see Table I for details). The figure shows the maximum of the relaxation function as a function of the squared magnetic field H^2. It is easy to estimate the slope at $H^2 = 0$ (from which ξ is measured) for the 1999 data, which display a linear behavior for $H^2 \lesssim 6 \times 10^4$ Oe^2. Instead, the large ξ of the 2020 data not only causes a larger slope, but also a much larger curvature (see the zoomed in region in the **inset**) which makes it challenging to extrapolate the slope to $H^2 = 0$.

FIG. 2. A set of relaxation curves $S(t) = d(M/H)/d\ln t$ for CuMn at $T = 29$ K and $t_w = 10^4$ s (**top**) and for the Ising-Edwards-Anderson model at $T = 0.9$ and $t_w = 2^{22}$ lattice sweeps (**bottom**). The relation between IEA and physical units is discussed in the text.

a scaling law that describes the system's response over its entire natural range of variation.

To be specific, let us consider the zero-field-cooled protocol (see, e.g., [20]), where the spin glass is suddenly quenched from a temperature well above T_g down to the working temperature $T_m < T_g$ and is then left to relax for a time t_w [the growth of the correlation length $\xi(t_w)$ is unbounded for $T < T_g$, but very slow]. At time t_w, a magnetic field H is applied and the growing magnetization $M(t, t_w; H)$ is recorded for times $t + t_w$ (the t_w dependence is included because spin glasses perennially age at $T < T_g$, slowly approaching equilibrium but never reaching it). The maximum of the relaxation function $d(M/H)/d\ln t$ defines a time t_H^{eff} directly related to the height of the free-energy barriers that the system encounters. In a magnetic field, the Zeeman effect lowers these barriers by an amount proportional to H^2 and to the number of spins in a glassy cluster. Therefore, an Arrhenius law would predict a linear behavior of $\ln t_H^{eff}$ with H^2. Yet, see Fig. 1, departures from a straight line were observed for large values of H^2 in the very first experiment using this approach [16]. In fact, the Zeeman interpretation has been disputed [17, 22] and identifying a linear behavior in H^2 becomes problematic close to T_g [20].

In what follows, we shall derive a scaling law for the response to the magnetic field that is still valid for large fields and close to T_g. As we stated above, the scaling law is tested against measurements in a single CuMn crystal
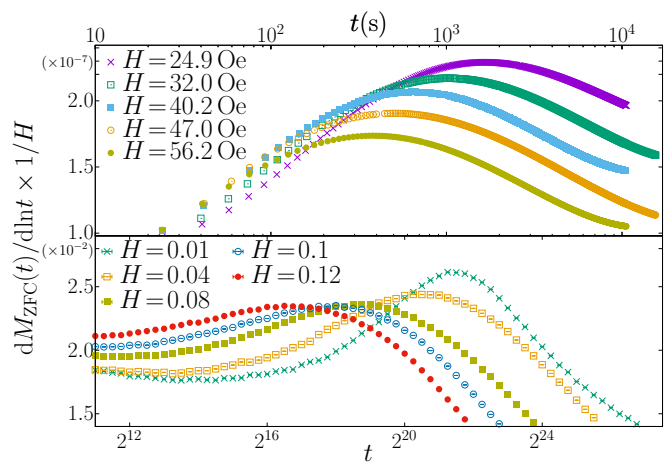
and against massive numerical simulations carried out on Janus II. The single crystal is important because the growth of $\xi(t_w)$ is not limited like in a poly-crystal with grain boundaries [23]. Specifically, we shall show that the H dependence has the form

$$\ln \frac{t_H^{eff}}{t_{H\to 0^+}^{eff}} = \frac{\hat{S}}{T}\xi^{D-\frac{\theta}{2}}H^2 \; + \; \xi^{-\theta/2}\mathcal{G}\big(\xi^{D-\frac{\theta}{2}}H^2; T\big). \quad (1)$$

Here ξ stands for $\xi(t_w)$, $\hat{S}$ is a constant, $D = 3$ is the spatial dimension and θ stands for the replicon exponent $\theta(\tilde{x})$ [4–6], where $\tilde{x} = \ell_J(T)/\xi(t_w)$ and $\ell_J(T)$ is the Josephson length [13, 20].

For small values of x the scaling function behaves as $\mathcal{G}(x) \sim x^2$ ($x = \xi^{D-\frac{\theta}{2}}H^2$). Hence, $\mathcal{G}$ is of order H^4 for small values of the magnetic field and, if ξ is small (the typical case well below T_g), the contribution of $\mathcal{G}$ can be neglected for small H. In fact, most previous experiments and simulations only tested the H^2 term in Eq. (1). We find here, however, that for larger fields, or larger correlation lengths (which are found only close to T_g), $\mathcal{G}$ is the dominant contribution. Fortunately, Eq. (1) offers a unified framework that rationalizes the entire range of experiment and simulations.

Experimental and numerical descriptions. Our experiments used a commercial DC SQUID to measure the magnetization of a $Cu_{94}Mn_6$ single crystal with $T_g = 31.5$ K, grown at Ames Laboratory, U.S. DOE (see [20] for details). The sample was quenched from 40 K at 10 K/min to the measuring temperature T_m in zero magnetic field. After the temperature was stabilized, the system was aged for a waiting time t_w before a magnetic field H was turned on, and the magnetization $M_{ZFC}(t, t_w; T_m)$ was recorded as a function of time t. The temperatures were chosen as 28.5 K, 28.75 K and 29 K, so $T_m \geq 0.9T_g$. The magnetic fields ranged from 16 Oe to 59 Oe. Table I

	T_{m} (K)	t_{w} (s)	$\xi(t_{\mathrm{w}})/a$	$\theta(\tilde{x})$
Exp. 1	28.50	10 000	320.36	0.337
Exp. 2	28.75	10 000	341.76	0.344
Exp. 3	28.75	20 000	359.18	0.342
Exp. 4	29.00	10 000	391.27	0.349

TABLE I. Main parameters for our four experiments, including the correlation length at time t_{w} (in units of the average Mn-Mn spacing a) and the effective replicon exponent $\theta(\tilde{x})$, obtained from the interpolation in [20] of the results in [13].

	T_{m}	t_{w}	$\xi(t_{\mathrm{w}}, H=0)$	$\theta(\tilde{x})$	C_{peak}
Run 1	0.9	2^{22}	8.294(7)	0.455	0.530
Run 2	0.9	$2^{26.5}$	11.72(2)	0.436	0.510
Run 3	0.9	$2^{31.25}$	16.63(5)	0.415	0.490
Run 4	1.0	$2^{23.75}$	11.79(2)	0.512	0.419
Run 5	1.0	$2^{27.625}$	16.56(5)	0.498	0.400
Run 6	1.0	$2^{31.75}$	23.63(14)	0.484	0.383

TABLE II. Main parameters for our numerical simulations, including the replicon exponent $\theta(\tilde{x})$ and the value of C_{peak} employed in Eq. (3).

shows the relevant experimental parameters, including the effective replicon exponent $\theta(\tilde{x})$.

In parallel with these experiments, we have simulated the Ising-Edwards-Anderson (IEA) model, with Hamiltonian $\mathcal{H} = -\sum_{\langle \boldsymbol{x}, \boldsymbol{y} \rangle} J_{\boldsymbol{x}\boldsymbol{y}} s_{\boldsymbol{x}} s_{\boldsymbol{y}} - H \sum_{\boldsymbol{x}} s_{\boldsymbol{x}}$, where $s_{\boldsymbol{x}} = \pm 1$ is the spin at site $\boldsymbol{x}$. We have used one sample of a cubic lattice with periodic boundary conditions, linear size $L = 160$ and random couplings $J_{\boldsymbol{x}\boldsymbol{y}} = \pm 1$ [24]. In these natural units, and for $H = 0$, the IEA model undergoes a spin-glass phase transition at the critical temperature $T_{\mathrm{g}} = 1.102(3)$ [25]. We simulated the non-equilibrium dynamics by means of a Metropolis algorithm. The natural time unit is the lattice sweep, which roughly corresponds to one picosecond of physical time. As for the magnetic field, Ref. [12] estimated from experimental $Fe_{0.5}Mn_{0.5}TiO_3$ data [26] that $H = 1$ in the IEA model corresponds to 5×10^4 Oe.

In order to mimic the experimental setup in the simulations, an initial random spin configuration is placed instantaneously at the working temperature T_{m} and left to relax for a time t_{w}, with $H = 0$. At time t_{w}, the external magnetic field is turned on and the magnetization $M(t, t_{\mathrm{w}}; H)$ and the correlation function $C(t, t_{\mathrm{w}}; H) = \sum_{\boldsymbol{x}} s_{\boldsymbol{x}}(t_{\mathrm{w}}; H=0) s_{\boldsymbol{x}}(t + t_{\mathrm{w}}; H)/160^3$ are recorded.

Our experimental range (16 Oe to 59 Oe) corresponds to $0.0003 \lesssim H \lesssim 0.0012$ in the IEA model, but the signal-to-noise ratio limited our simulations to $H \geq 0.005$. We employed two tricks to match these scales. On the one hand, we can use dimensional analysis [27] to relate H and the reduced temperature $\hat{t} = (T_{\mathrm{g}} - T)/T_{\mathrm{g}}$ through

$$\hat{t}_{\mathrm{num}} \approx \hat{t}_{\mathrm{exp}} \left(\frac{H_{\mathrm{num}}}{H_{\mathrm{exp}}} \right)^{\frac{4}{\nu(5-\eta)}}, \quad (2)$$

where $\nu = 2.56(4)$ and $\eta = -0.390(4)$ are $H = 0$ critical exponents [25], while the subscripts exp and num stand for experiment and simulation. Eq. (2) suggests that we increase $\hat{t}_{\mathrm{num}}$ to reach the experimental scale with our range or H_{num}, which results in $0.89 \lesssim T_{\mathrm{num}} \lesssim 0.99$. Given our pre-existing database of long simulations at $H = 0$ [13], it has been convenient to work at temperatures $T_{\mathrm{m}} = 0.9$ and $T_{\mathrm{m}} = 1.0$ (or $\hat{t} = 0.183$ and 0.093).

On the other hand, we have found that, when $H \to 0$, the correlation function $C(t, t_{\mathrm{w}}; H)$ approaches a constant value C_{peak} at the maximum of the relaxation function [28], which suggests computing t_H^{eff} in the simulations

from the equation

$$C(t_H^{\mathrm{eff}}, t_{\mathrm{w}}; H) = C_{\mathrm{peak}}. \quad (3)$$

See [29] for a similar choice in an equilibrium context. This is helpful because Eq. (3) can be solved at $H = 0$ as well [in contrast with the magnetization, $C(t, t_{\mathrm{w}}; H)$ does not vanish at $H = 0$]. The values of C_{peak} are given in Table II.

The scaling law. We work here on the same assumptions of Ref. [12], though we shall be able to improve on their findings.

In equilibrium and for large-enough correlation lengths, a scaling theory describes the magnetic response to an external field H [30, 31]. Our assumption will be (see also Refs. [10, 11]) that this scaling theory holds as well in the non-equilibrium regime, at least for large $\xi(t_{\mathrm{w}})$ and small H:

$$M(t, t_{\mathrm{w}}; H) = [\xi(t + t_{\mathrm{w}})]^{-\frac{D}{2} - \frac{\theta(\tilde{x})}{4}}$$
$$\times \mathcal{F}\left(H[\xi(t + t_{\mathrm{w}})]^{\frac{D}{2} - \frac{\theta(\tilde{x})}{4}}, \frac{\xi(t + t_{\mathrm{w}})}{\xi(t_{\mathrm{w}})} \right), \quad (4)$$

Because of (at least approximate) full-aging spin-glass dynamics (see, e.g., [32]), Eq. (3) tells us that $\xi(t + t_{\mathrm{w}})/\xi(t_{\mathrm{w}})$ will be approximately constant close to the maximum of the relaxation rate (see Fig. 2), and we shall omit this dependence. Taylor expanding Eq. (4), and recalling that $\mathcal{F}(x) = -\mathcal{F}(-x)$, we find

$$M(t, t_{\mathrm{w}}; H) = \chi_1 H + \frac{\chi_3}{3!} H^3 + \frac{\chi_5}{5!} H^5 + \mathcal{O}(H^7), \quad (5)$$

where [33]

$$\chi_{2n-1} \propto b_{2n}(T)[\xi(t_{\mathrm{w}})]^{(n-1)D - \frac{n\theta(\tilde{x})}{2}} \quad (6)$$

[$b_{2n}(T)$ is a smooth function of T].

Our improvements over the results of [12] start from the observation that Eq. (6) predicts the paradoxical result $\chi_1 \propto \xi^{-\theta(\tilde{x})/2}$ (hence, χ_1 would go to zero when $\xi \to \infty$). In fact, Eq. (6) neglects the contribution of the regular part of the free energy. A better description, then, is

$$\chi_1 = \frac{\hat{S}(C_{\mathrm{peak}})}{T} + \frac{b_2(T)}{\xi^{\theta(\tilde{x})/2}}, \quad (7)$$

where $\hat{S}\big(C(t,t_{\mathrm{w}})\big)$ is the function appearing in the fluctuation-dissipation relations (FDR) [34–37] [from now on, we use the shorthand $\hat{S}$ for $\hat{S}(C_{\mathrm{peak}})$].

Our next assumption will be that we can determine the excess free energy per spin in a field as it is done in equilibrium (by integrating M with respect to H)

$$\Delta F = -\left[\frac{\chi_1}{2}H^2 + \frac{\chi_3}{4!}H^4 + \frac{\chi_5}{6!}H^6 + \mathcal{O}(H^8)\right]. \quad (8)$$

Eq. (8), combined with Eqs. (6,7) leads directly to Eq. (1) when one makes a few additional hypothesis [38]: (i) according to an Arrhenius law, see [16, 22, 39], $t_H^{\mathrm{eff}}/t_{H=0}^{\mathrm{eff}} = \exp[N\Delta F/(k_{\mathrm{B}}T)]$ where N is the number of spins in a glassy domain, and (ii) $N \propto \xi^{D-\theta(\tilde{x})/2}$ [12].

The prefactor $\xi^{-\theta(\tilde{x})/2}$ for the $\mathcal{G}$ term in Eq. (1), not included in Ref. [12], will be crucial here because, unlike in [12], we shall test Eq. (1) in situations where the $\mathcal{G}$ term is the dominant contribution.

Experimental and numerical results. We look at relaxation function curves exhibited in Fig. 2, from which the effective times t_H^{eff} are obtained. Our results for $\ln t_H^{\mathrm{eff}}$ (experiment) and $\ln t_H^{\mathrm{eff}}/t_{H=0}^{\mathrm{eff}}$ (simulations) are displayed in Fig. 3. The technical details about this analysis will appear elsewhere [28]. Both the experimental and the numerical data in Fig. 3 deviate very significantly from linear behavior, which suggests that the $\mathcal{G}$ term in Eq. (1) is, indeed, playing a dominant role.

Our next step is fitting the experimental data to

$$\ln t_H^{\mathrm{eff}} = a_0 + a_2 H^2 + a_4 H^4 + a_6 H^6 + \mathcal{O}(H^8). \quad (9)$$

Note that, in the experiments, $\ln t_H^{\mathrm{eff}}$ needs to be extrapolated to $H = 0$ (this is the meaning of the a_0 term). Our coefficients a_n are listed in Table III. We extract ξ from the a_2 term as explained in Ref. [20]. For the higher-order terms, Eqs. (1,5) predict $a_n \propto b_{2n}(T)\xi^{[nD-(n+1)\theta(\tilde{x})]/2}$. For instance, the $T = 28.75$ K data with $t_{\mathrm{w}}^{(1)} = 10$ ks and $t_{\mathrm{w}}^{(2)} = 20$ ks allow a direct test of the scaling relation. Taking for $\theta(\tilde{x})$ the average value $\theta = 0.343$ [28] we find

$$\xi(t_{\mathrm{w}}^{(2)})/\xi(t_{\mathrm{w}}^{(1)}) = \left[a_2(t_{\mathrm{w}}^{(2)})/a_2(t_{\mathrm{w}}^{(1)})\right]^{\frac{1}{D-\theta/2}} = 1.053,$$

$$\xi(t_{\mathrm{w}}^{(2)})/\xi(t_{\mathrm{w}}^{(1)}) = \left[a_4(t_{\mathrm{w}}^{(2)})/a_4(t_{\mathrm{w}}^{(1)})\right]^{\frac{1}{2D-\frac{3\theta}{2}}} = 1.048, \quad (10)$$

$$\xi(t_{\mathrm{w}}^{(2)})/\xi(t_{\mathrm{w}}^{(1)}) = \left[a_6(t_{\mathrm{w}}^{(2)})/a_6(t_{\mathrm{w}}^{(1)})\right]^{\frac{1}{3D-2\theta}} = 1.052.$$

We can, therefore, gain access to the $\mathcal{G}$ term in Eq. (1) by subtracting $a_0 + a_2 H^2$ from the experimental value of $\ln t_H^{\mathrm{eff}}$.

As for the numerical data, polynomial fits analogous to Eq. (9) are possible, but result in wildly oscillating curves. The simplest explanation for this behavior is that our largest magnetic fields are beyond the radius of convergence of the Taylor expansion of Eq. (1). One can, however, compute a_2 by estimating the derivative of $\ln(t_H^{\mathrm{eff}}/t_{H\to 0^+}^{\mathrm{eff}})$ numerically at $H^2 = 0$ [28]. Hence, we can access the $\mathcal{G}$ term in Eq. (1) with the same subtraction that we used for the experimental data.
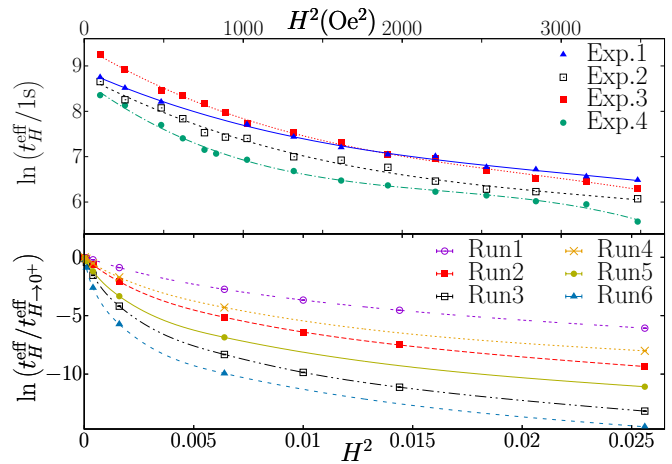

FIG. 3. Experimental and numerical $\ln t_{\mathrm{w}}^{\mathrm{eff}}$ from the maximum of the response function in Fig. 2. **Top**: Data from the experiments in Table I. Lines are fits to a polynomial in H^2, as in Eq. (9). The fit parameters are reported in Table III. **Bottom**: Numerical data for the runs in Table II (the lines are just guides for the eye).

T_{m} (K)	t_{w}(s)	coefficient	value
28.5	10000	a_2	$-1.551 \times 10^{-3} \pm 1.03 \times 10^{-4}$
		a_4	$3.980 \times 10^{-7} \pm 6.99 \times 10^{-8}$
		a_6	$-4.363 \times 10^{-11} \pm 1.29 \times 10^{-11}$
28.75	10000	a_2	$-1.816 \times 10^{-3} \pm 2.00 \times 10^{-4}$
		a_4	$4.565 \times 10^{-7} \pm 1.32 \times 10^{-7}$
		a_6	$-4.584 \times 10^{-11} \pm 2.45 \times 10^{-11}$
28.75	20000	a_2	$-2.104 \times 10^{-3} \pm 1.19 \times 10^{-4}$
		a_4	$5.889 \times 10^{-7} \pm 7.88 \times 10^{-8}$
		a_6	$-7.013 \times 10^{-11} \pm 1.47 \times 10^{-11}$
29	10000	a_2	$-2.609 \times 10^{-3} \pm 1.28 \times 10^{-4}$
		a_4	$1.016 \times 10^{-6} \pm 8.45 \times 10^{-8}$
		a_6	$-1.491 \times 10^{-10} \pm 1.57 \times 10^{-11}$

TABLE III. Experimental data: coefficients a_n of the polynomial fit of $\ln t_{\mathrm{w}}^{\mathrm{eff}}$, see Eq. (9), as a function of T_{m} and t_{w}.

Finally, Fig. 4 brings these analyses together to perform a strong test of Eq. (1) (assuming that the coefficients b_4 and b_6 are almost constant in the temperature range of interest). The agreement with the scaling prediction, manifested in a data collapse, is striking both for the experimental and the numerical data [40].

Conclusions. The melding of experiment, theory and simulations, as exhibited in Figs. (2)–(4), is a spectacular success of statistical mechanics. If the right questions are asked, a truly schematic model (namely the Ising-Edwards-Anderson model) turns out to behave, quantitatively, in the same way that CuMn does. The crucial ingredients to uncover this universal behavior have been high-quality simulations carried out on a custom-built computer, careful experiments capable of addressing the relevant regime of very large correlation lengths close to the glass temperature, and an extension to the
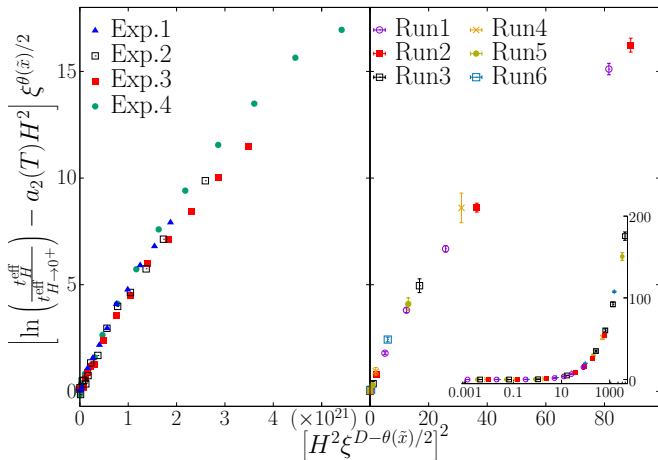
FIG. 4. The non-linear part of the response time data: $[\ln(t_H^{\text{eff}}/t_{H\to 0^+}^{\text{eff}}) - a_2(T)H^2]\xi^{\theta(\tilde{x})/2}$ plotted against the scaling variable $[H^2\xi^{D-\theta(\tilde{x})/2}]^2$, see Eq. (1). **Left**: Experimental data (see Table I). **Right**: Numerical data (see Table II). The **main panel**, in linear scale, shows a closeup for small values of $[H^2\xi^{D-\theta(\tilde{x})/2}]^2$. The **inset** is in log scale in order to report all our numerical data. Note that experimental and numerical data are reported in different unit systems (see main text).

non-equilibrium context of the classical equilibrium scaling theory. We are now able to model quantitatively —in a framework that encompasses both experiments and numerical simulations— responses, autocorrelation lengths, and energy barriers in three-dimensional spin glasses. This will allow us to address more exotic phenomena such as rejuvenation (temperature chaos) and memory effects. Moreover, because spin glasses are influential in so many other fields (such as econophysics, biology or optimization in computer science), our work shows that successful modeling of complex systems is feasible in finite dimensions.

ACKNOWLEDGMENTS

Appendix A: Comparison between different non-linear scaling laws

In the main text, we introduced the non-linear scaling law (1), that we argued represents a significant step forward in Ref. [12].

In order to give a better sense of the improvement achieved through Eq. (1), we show here that the data do not collapse equally well if we use two different scaling laws, one from Ref. [12] and the other a simple rational modification of Ref. [12]. Specifically, we reanalyze our data both through the scaling equation proposed in Ref. [12],

$$\ln \frac{t_H^{\text{eff}}}{t_{H\to 0^+}^{\text{eff}}} = \mathcal{F}\left(\xi^{D-\frac{\theta(\tilde{x})}{2}}H^2\right), \tag{A1}$$

or by postulating that the data can be rationalized through a single scaling term,

$$\left[\ln \frac{t_H^{\text{eff}}}{t_{H\to 0^+}^{\text{eff}}}\right]\xi^{\theta(\tilde{x})/2} = \mathcal{F}\left(\xi^{D-\frac{\theta(\tilde{x})}{2}}H^2\right). \tag{A2}$$

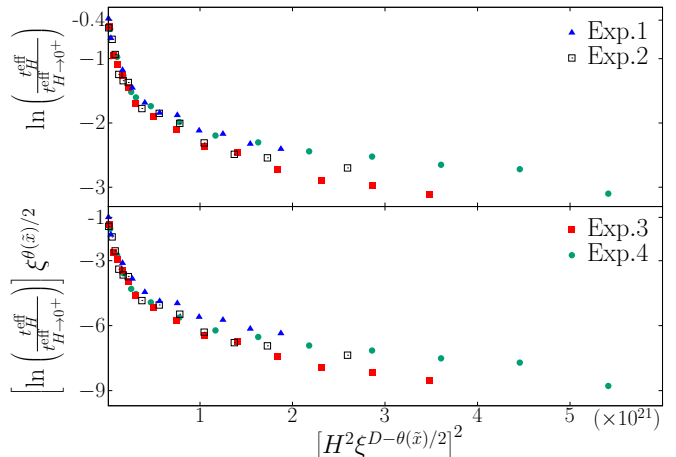We report the non-linear scaling behaviors using Eqs. (A1) and (A2) in Figs. 5 (experimental data) and 6

FIG. 5. **Top** The non-linear part of the experimental response time data: $[\ln(t_H^{\text{eff}}/t_{H\to 0^+}^{\text{eff}})$ plotted against the scaling variable $[H^2\xi^{D-\theta(\tilde{x})/2}]^2$, according to Ref. [12], see Eq. (A1). The plot is in linear scale. **Bottom** The non-linear part of the response time data:$[\ln(t_H^{\text{eff}}/t_{H\to 0^+}^{\text{eff}})\xi^{\theta(\tilde{x})/2}$ plotted against the scaling variable $[H^2\xi^{D-\theta(\tilde{x})/2}]^2$, according to Eq. (A2). The plot is in linear scale.

(numerical data). To ease comparisons, we use the same scaling variable and x-axis scale that we used in Fig. 4 of the main text, where we collapsed the data using Eq. (1). However, because the scalings are easier to interpret with a linear y-axis scale, we also provide the same plots in a semi-log scale (Figs. 7 and 8).

The collapse of the experimental data with Eqs. (A1) and (A2) (Figs. 5 and 7) works well only at most $x = (H^2\xi^{D-\theta/2})^2 = 6\times 10^{20}\,\mathrm{Oe}$, which is about half of the validity range of the collapses in Fig. 4 of the main text, which are accurate at least up to $x = 2\times 10^{21}\,\mathrm{Oe}$.

The collapse of the numerical data with Eqs. (A1) and (A2) (Figs. 6 and 8) is less accurate throughout the whole range of x.

We believe, therefore, that the scaling relationship represented by Eq. 1, taken from the main text, is far superior.
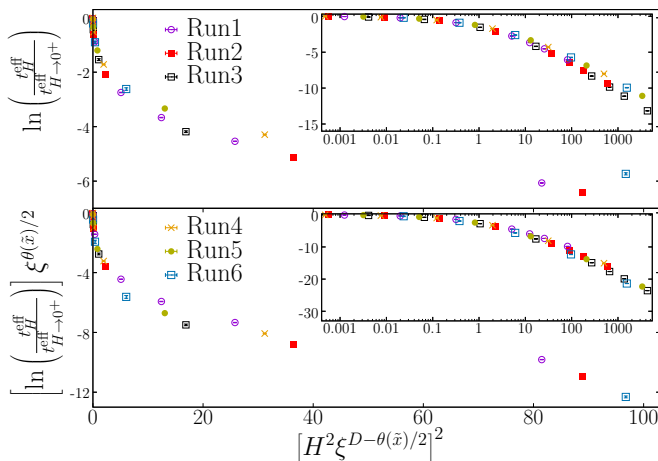

FIG. 6. **Top** The non-linear part of the numerical response time data: $[\ln(t_H^{\mathrm{eff}}/t_{H\to 0^+}^{\mathrm{eff}})$ plotted against the scaling variable $[H^2\xi^{D-\theta(\tilde{x})/2}]^2$, according to Ref. [12], see Eq. (A1). Its **main** panel is in linear scale, instead its **insert** is in semi-log scale. **Bottom** The non-linear part of the response time data: $[\ln(t_H^{\mathrm{eff}}/t_{H\to 0^+}^{\mathrm{eff}})\xi^{\theta(\tilde{x})/2}$ plotted against the scaling variable $[H^2\xi^{D-\theta(\tilde{x})/2}]^2$, according to Eq. (A2). Its **main** panel is in linear scale, instead its **insert** is in semi-log scale.
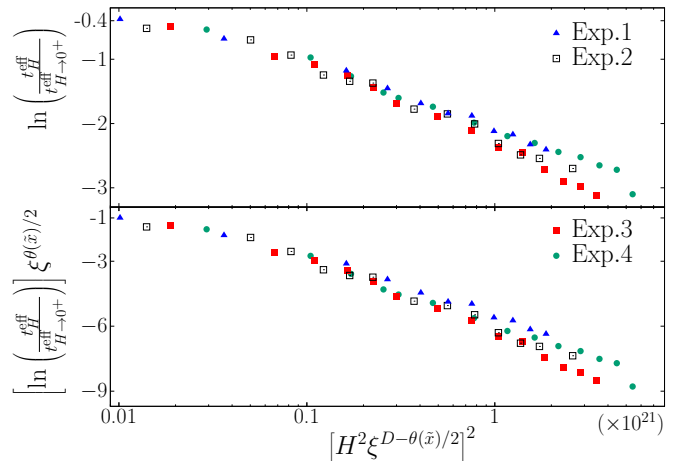

FIG. 7. **Top** The non-linear part of the experimental response time data: $[\ln(t_H^{\mathrm{eff}}/t_{H\to 0^+}^{\mathrm{eff}})$ plotted against the scaling variable $[H^2\xi^{D-\theta(\tilde{x})/2}]^2$, according to Ref. [12], see Eq. (A1). The plot is in semi-log scale. **Bottom** The non-linear part of the response time data: $[\ln(t_H^{\mathrm{eff}}/t_{H\to 0^+}^{\mathrm{eff}})\xi^{\theta(\tilde{x})/2}$ plotted against the scaling variable $[H^2\xi^{D-\theta(\tilde{x})/2}]^2$, according to Eq. (A2). The plot is in semi-log scale.
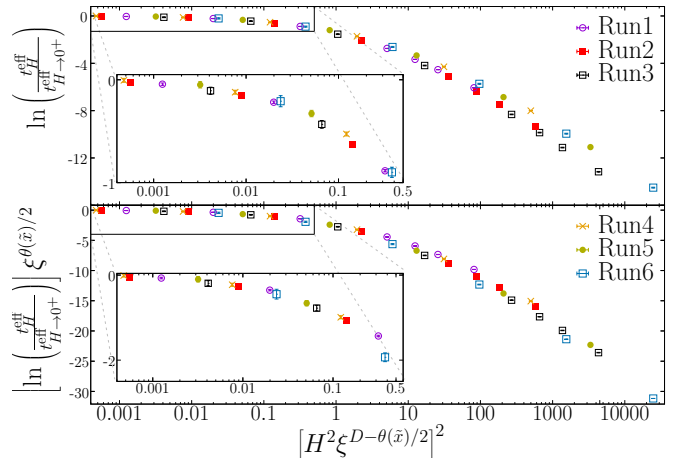

FIG. 8. **Top** The non-linear part of the numerical response time data: $[\ln(t_H^{\mathrm{eff}}/t_{H\to 0^+}^{\mathrm{eff}})$ plotted against the scaling variable $[H^2\xi^{D-\theta(\tilde{x})/2}]^2$, according to Ref. [12], see Eq. (A1). Its **main** panel is in semi-log scale and its **insert** is a zoom in the small x region. **Bottom** The non-linear part of the response time data: $[\ln(t_H^{\mathrm{eff}}/t_{H\to 0^+}^{\mathrm{eff}})\xi^{\theta(\tilde{x})/2}$ plotted against the scaling variable $[H^2\xi^{D-\theta(\tilde{x})/2}]^2$, according to Eq. (A2). Its **main** panel is in semi-log scale and its **insert** is a zoom in the small x range.

[1] A. Cavagna, Physics Reports **476**, 51 (2009), arXiv:0903.4264.

[2] P. Charbonneau, J. Kurchan, G. Parisi, P. Urbani, and F. Zamponi, Nature Communications **5**, 3725 (2014), arXiv:1404.6809.

[3] G. Adam and J. H. Gibbs, The Journal of Chemical Physics **43**, 139 (1965).

[4] E. Marinari, G. Parisi, J. Ruiz-Lorenzo, and F. Ritort,

Phys. Rev. Lett. **76**, 843 (1996).

[5] F. Belletti, M. Cotallo, A. Cruz, L. A. Fernandez, A. Gordillo-Guerrero, M. Guidetti, A. Maiorano, F. Mantovani, E. Marinari, V. Martín-Mayor, A. M. Sudupe, D. Navarro, G. Parisi, S. Perez-Gaviro, J. J. Ruiz-Lorenzo, S. F. Schifano, D. Sciretti, A. Tarancon, R. Tripiccione, J. L. Velasco, and D. Yllanes (Janus Collaboration), Phys. Rev. Lett. **101**, 157201 (2008), arXiv:0804.1471.

[6] F. Belletti, A. Cruz, L. A. Fernandez, A. Gordillo-Guerrero, M. Guidetti, A. Maiorano, F. Mantovani, E. Marinari, V. Martín-Mayor, J. Monforte, A. Muñoz Sudupe, D. Navarro, G. Parisi, S. Perez-Gaviro, J. J. Ruiz-Lorenzo, S. F. Schifano, D. Sciretti, A. Tarancon, R. Tripiccione, and D. Yllanes (Janus Collaboration), J. Stat. Phys. **135**, 1121 (2009), arXiv:0811.2864.

[7] R. Alvarez Baños, A. Cruz, L. A. Fernandez, J. M. Gil-Narvion, A. Gordillo-Guerrero, M. Guidetti, A. Maiorano, F. Mantovani, E. Marinari, V. Martín-Mayor, J. Monforte-Garcia, A. Muñoz Sudupe, D. Navarro, G. Parisi, S. Perez-Gaviro, J. J. Ruiz-Lorenzo, S. F. Schifano, B. Seoane, A. Tarancon, R. Tripiccione, and D. Yllanes (Janus Collaboration), Phys. Rev. Lett. **105**, 177202 (2010), arXiv:1003.2943.

[8] M. Manssen and A. K. Hartmann, Phys. Rev. B **91**, 174433 (2015), arXiv:1411.5512.

[9] M. Manssen, A. K. Hartmann, and A. P. Young, Phys. Rev. B **91**, 104430 (2015), arXiv:1501.06760.

[10] L. A. Fernández and V. Martín-Mayor, Phys. Rev. B **91**, 174202 (2015).

[11] M. Lulli, G. Parisi, and A. Pelissetto, Phys. Rev. E **93**, 032126 (2016).

[12] M. Baity-Jesi, E. Calore, A. Cruz, L. A. Fernandez, J. M. Gil-Narvion, A. Gordillo-Guerrero, D. Iñiguez, A. Maiorano, E. Marinari, V. Martin-Mayor, J. Monforte-Garcia, A. Muñoz Sudupe, D. Navarro, G. Parisi, S. Perez-Gaviro, F. Ricci-Tersenghi, J. J. Ruiz-Lorenzo, S. F. Schifano, B. Seoane, A. Tarancon, R. Tripiccione, and D. Yllanes (Janus Collaboration), Phys. Rev. Lett. **118**, 157202 (2017).

[13] M. Baity-Jesi, E. Calore, A. Cruz, L. A. Fernandez, J. M. Gil-Narvion, A. Gordillo-Guerrero, D. Iñiguez, A. Maiorano, E. Marinari, V. Martin-Mayor, J. Moreno-Gordo, A. Muñoz Sudupe, D. Navarro, G. Parisi, S. Perez-Gaviro, F. Ricci-Tersenghi, J. J. Ruiz-Lorenzo, S. F. Schifano, B. Seoane, A. Tarancon, R. Tripiccione, and D. Yllanes (Janus Collaboration), Phys. Rev. Lett. **120**, 267203 (2018).

[14] L. A. Fernandez, E. Marinari, V. Martin-Mayor, I. Paga, and J. J. Ruiz-Lorenzo, Phys. Rev. B **100**, 184412 (2019).

[15] S. Albert, T. Bauer, M. Michl, G. Biroli, J.-P. Bouchaud, A. Loidl, P. Lunkenheimer, R. Tourbot, C. Wiertel-Gasquet, and F. Ladieu, Science **352**, 1308 (2016), arXiv:1606.04079.

[16] Y. G. Joh, R. Orbach, G. G. Wood, J. Hammann, and E. Vincent, Phys. Rev. Lett. **82**, 438 (1999).

[17] F. Bert, V. Dupuis, E. Vincent, J. Hammann, and J.-P. Bouchaud, Phys. Rev. Lett. **92**, 167203 (2004).

[18] S. Guchhait and R. Orbach, Phys. Rev. Lett. **112**, 126401 (2014).

[19] S. Guchhait and R. L. Orbach, Phys. Rev. Lett. **118**, 157203 (2017).

[20] Q. Zhai, V. Martin-Mayor, D. L. Schlagel, G. G. Kenning, and R. L. Orbach, Phys. Rev. B **100**, 094202 (2019).

[21] M. Baity-Jesi, R. A. Baños, A. Cruz, L. A. Fernandez, J. M. Gil-Narvion, A. Gordillo-Guerrero, D. Iniguez, A. Maiorano, F. Mantovani, E. Marinari, V. Martín-Mayor, J. Monforte-Garcia, A. Muñoz Sudupe, D. Navarro, G. Parisi, S. Perez-Gaviro, M. Pivanti, F. Ricci-Tersenghi, J. J. Ruiz-Lorenzo, S. F. Schifano, B. Seoane, A. Tarancon, R. Tripiccione, and D. Yllanes (Janus Collaboration), Comp. Phys. Comm **185**, 550 (2014), arXiv:1310.1032.

[22] E. Vincent, J. P. Bouchaud, D. S. Dean, and J. Hammann, Phys. Rev. B **52**, 1050 (1995).

[23] G. G. Kenning, D. M. Tennant, C. M. Rost, F. G. da Silva, B. J. Walters, Q. Zhai, D. C. Harrison, E. D. Dahlberg, and R. L. Orbach, Phys. Rev. B **98**, 104436 (2018).

[24] In a $L = 160$ system, $\xi(t_w)$ and $M(t, t_w; H)$ display little sample dependence, see [28]. We have, however, run 512 independent thermal histories for our sample (the benefits of simulating many independent thermal histories are discussed in Ref. [13]).

[25] M. Baity-Jesi, R. A. Baños, A. Cruz, L. A. Fernandez, J. M. Gil-Narvion, A. Gordillo-Guerrero, D. Iniguez, A. Maiorano, F. Mantovani, E. Marinari, V. Martín-Mayor, J. Monforte-Garcia, A. Muñoz Sudupe, D. Navarro, G. Parisi, S. Perez-Gaviro, M. Pivanti, F. Ricci-Tersenghi, J. J. Ruiz-Lorenzo, S. F. Schifano, B. Seoane, A. Tarancon, R. Tripiccione, and D. Yllanes (Janus Collaboration), Phys. Rev. B **88**, 224416 (2013), arXiv:1310.2910.

[26] H. Aruga Katori and A. Ito, Journal of the Physical Society of Japan **63**, 3122 (1994), http://dx.doi.org/10.1143/JPSJ.63.3122.

[27] D. S. Fisher and H. Sompolinsky, Phys. Rev. Lett. **54**, 1063 (1985).

[28] Q. Zhai, D. L. Schlagel, R. L. Orbach, I. Paga, M. Baity-Jesi, E. Calore, A. Cruz, L. A. Fernandez, J. M. Gil-Narvion, I. González-Adalid Pemartín, A. Gordillo-Guerrero, D. Iñiguez, A. Maiorano, E. Marinari, V. Martin-Mayor, J. Moreno-Gordo, A. Muñoz Sudupe, D. Navarro, G. Parisi, S. Perez-Gaviro, F. Ricci-Tersenghi, J. J. Ruiz-Lorenzo, S. F. Schifano, B. Seoane, A. Tarancon, R. Tripiccione, and D. Yllanes, (2020), manuscript in preparation.

[29] I. González-Adalid Pemartín, V. Martin-Mayor, G. Parisi, and J. J. Ruiz-Lorenzo, Journal of Physics A: Mathematical and Theoretical **52**, 134002 (2019).

[30] G. Parisi, *Statistical Field Theory* (Addison-Wesley, 1988).

[31] D. J. Amit and V. Martín-Mayor, *Field Theory, the Renormalization Group and Critical Phenomena*, 3rd ed. (World Scientific, Singapore, 2005).

[32] G. F. Rodriguez, G. G. Kenning, and R. Orbach, Phys. Rev. Lett. **91**, 037203 (2003).

[33] In order to not overburden the notation we have omitted the t and t_w arguments in the r.h.s. susceptibilities in Eq. (5).

[34] L. F. Cugliandolo and J. Kurchan, Phys. Rev. Lett. **71**, 173 (1993).

[35] E. Marinari, G. Parisi, F. Ricci-Tersenghi, and J. J. Ruiz-Lorenzo, Journal of Physics A: Mathematical and General **31**, 2611 (1998).

[36] S. Franz, M. Mézard, G. Parisi, and L. Peliti, Phys. Rev. Lett. **81**, 1758 (1998).

[37] M. Baity-Jesi, E. Calore, A. Cruz, L. A. Fernandez, J. M. Gil-Narvión, A. Gordillo-Guerrero, D. Iñiguez, A. Maiorano, E. Marinari, V. Martin-Mayor, J. Monforte-Garcia, A. Muñoz Sudupe, D. Navarro, G. Parisi, S. Perez-Gaviro, F. Ricci-Tersenghi, J. J. Ruiz-Lorenzo, S. F. Schifano, B. Seoane, A. Tarancón, R. Tripiccione, and D. Yllanes, Proceedings of the National Academy of Sciences **114**, 1838 (2017).

[38] For the sake of simplicity, we have neglected the correction of order $\xi^{-\theta/2}$ in the H^2 term in Eq. (1).

[39] C. Djurberg, J. Mattsson, and P. Nordblad, Europhysics Letters (EPL) **29**, 163 (1995).

[40] Note that the scaling form of Eq. (1) is *necessary* to obtain a good collapse. To support this, we show in the Appendix that the collapse of Fig. 4 deteriorates if one assumes different scaling behaviors.